An Optical Microstructural Model for Blown Polyethylene Films

J. M. BOIX,[1] E. BERNABEU,[1] C. BARBA[2]

[1] Departamento de Optica, Facultad de Ciencias Físicas, Universidad Complutense de Madrid, 28040 Madrid, Spain

[2] Centro de Microscopía Electrónica "Luis Brú," Universidad Complutense de Madrid, 28040 Madrid, Spain

ABSTRACT: This paper presents an optical microstructural model showing, the behavior of blown low-density polyethylene films as optical polymers (birefringence and anisotropy), at a structural level. The model is mainly based on a microstructural study involving the observation and analysis of increasingly smaller structures by transmission electron microscopy, POM, and X-ray diffraction, as a means of calculating the values of their orientation functions (the uniaxial approximation). These values enabled us to indicate graphically the most probable average position of the unit cell (the natural scale of our model) and hence of other crystalline structures. © 2000 John Wiley & Sons, Inc. J Appl Polym Sci 75: 1708–1720, 2000

Key words: polymer optics; low-density polyethylene; transmission electron microscopy; microstructural polymer studies

INTRODUCTION

The refractive, birefringent, and anisotropic properties of polymers have all been the subject of many experimental studies. Schael[1,2] reported a polarized refractive index method and applied it to a series of oriented polyethylene and isotactic polypropylene films. A polarized refractive index study was carried out on poly(ethylene terephthalate) (PET) by de Vries et al.[3] along with another one on birefringence in fibers.[4–8] A detailed study was published[9] comparing the experimentally measured refractive indices for uniaxial isotactic polypropylene samples with theoretical predictions based on molecular models and their polarizability tensors.

In 1981 a review of the polarized refractive index technique and its applications included a unique "fractional orientation" approach for quantifying the degree of orientation in polymers.[10] A number of papers have been published more recently.[11–15] In 1967, Janeschitz–Kriegl and Wales[16] derived dimensionless groups for the correlation of flow birefringence data. This property of polymeric materials has also been studied by a number of other authors.[17–19] However, despite the abundance of literature, there has been no explanation of these properties based on a structural model.

In this article, a microstructural model is established for blown low-density polyethylene films, as a means of explaining the macroscopic optical behavior of birefringence and anisotropy. This model was based on results of polarization optical microscopy (POM) and transmission electron microscopy (TEM), plus a wide-angle X-ray scanning (WAXS) study with the determination of orientation functions (uniaxial approximation). The aim is to present, on the basis of TEM results, a series of microstructures, whose sizes progressively diminish down to the unit cell, this being the natural scale of our model and where it is located.

EXPERIMENTAL

Starting Films

For experimental application, tubular blown low-density polyethylene films were chosen. These

Correspondence to: J. M. Boix.

Journal of Applied Polymer Science, Vol. 75, 1708–1720 (2000)
© 2000 John Wiley & Sons, Inc.

Table I Measurements by POM of Angle $2V_i$ ($i = \alpha$ or γ), with the Optical Sign and Crystallinity Degree (16)

Sample	X_c (%)	$2V_\alpha \pm 2°$	$2V_\gamma \pm 2°$	Optic Sign
A	31.5	86°	94°	Negative
B	44.9	61°	119°	Negative
C	45.6	79°	101°	Negative
D	47.1	65°	115°	Negative
E	49.1	81°	99°	Negative

Table II Values of the Three Refraction Indices from the Low-Density Polyethylene Samples Studied

Sample	n_α	n_β	n_γ
A	1.5362	1.5235	1.5125
B	1.4874	1.5095	1.5171
C	1.4880	1.5058	1.5178
D	1.4884	1.5089	1.5172
E	1.4801	1.5024	1.5187

were transformed using a Brabender (Hackensack, NJ) AEV-320 Blown extruder with an annular blown film die (ID, 2 cm; OD, 2.6 cm). Extrusion was carried out on a 50/2 L/D extruder at a screw speed of 60 rpm and temperatures ranging from 140°C to 225°C. The blow-up ratio was 2.5 and the frost-line height was 8 cm. Film thickness was controlled via roller drag speed, resulting in a thickness of around 50 μm. The base polymers used in this study were commercially available polyethylene resins (melt flow index between 0.2 and 7 dg/mL) prepared by Repsol Química of Spain. A set of five samples, labeled A, B, C, D, and E, were chosen. Their degree of crystallinity, X_c (%) was first evaluated by X-ray diffraction[20] (results shown in Table I).

Polarized Optical Microscopy

Polarized optical microscopy was performed on a Zeiss Axiophot apparatus in conoscopic mode (Thornwood, NY). All samples exhibited weak crystal biaxiality. The same microscope, in orthoscopic mode with crossed polarizer and analyzer, was used to photograph 2-μm-thick cross sections cut with a Leica model Ultracut E ultramicrotome (Deerfield, IL).

Refraction data were completed by determining the values of the third refraction index, using a Zeiss Ultrafot II microscope equipped with a Fedorov plaque [measuring the angles formed by the two optical axes ($2V_\alpha$)].

X-ray Diffractometry

Diffractometric analysis of polyethylene films was carried out by wide-angle X-ray spectrophotometry using an X-ray diffractometer from Unicam Instrument Ltd (Cambridge') with Ni-filtered CuK_α ($\lambda = 0.15418$ nm), from a tube operating at

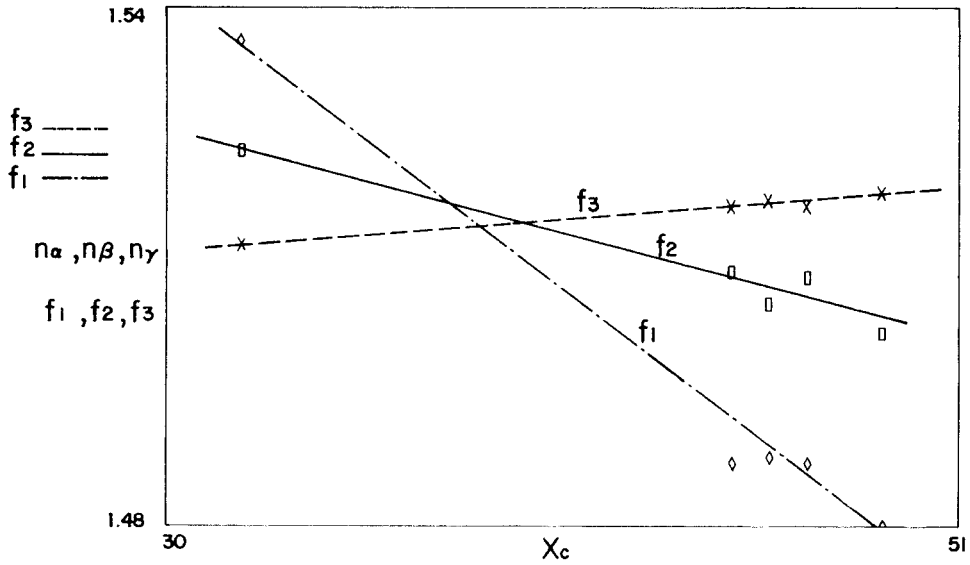

Figure 1 Graphic representation of the three refraction indices and their corresponding linear fittings, f_1, f_2, and f_3, versus the crystallinity degree for samples of LDPE. Here $n_\gamma \equiv n_0$ and $n_\beta \equiv n_e$. Their correlation coefficients are $e_1 = 0.9752$, $e_2 = 0.9756$, and $e_3 = 0.9886$, respectively.

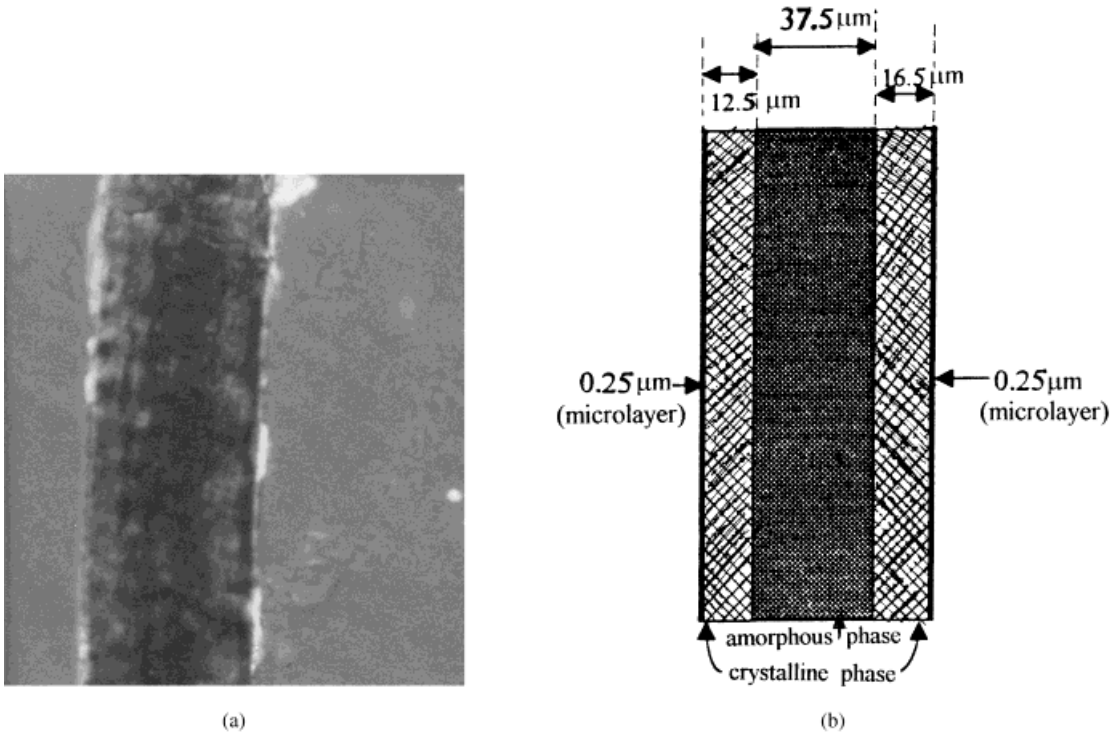

Figure 2 (a) Photograph taken by POM, with crossed polarizers, of a cut in a 2-μm-thick sample of blown polyethylene. (b) Schematic drawing of the previous cut, showing the limits of spatial distribution in low-density polyethylene films.

40 kV and 40 mA. Diffractograms were obtained at room temperature with an exposure time of 36 h and a distance of 40 mm between sample and film, which was placed perpendicular to the beam direction.

The method of R. S. Stein[21] can be used to calculate the values of the orientation functions f_α, f_β, and f_θ, indicating the average values of the angles forming the three crystallographic axes of a random crystal with respect to a predefined

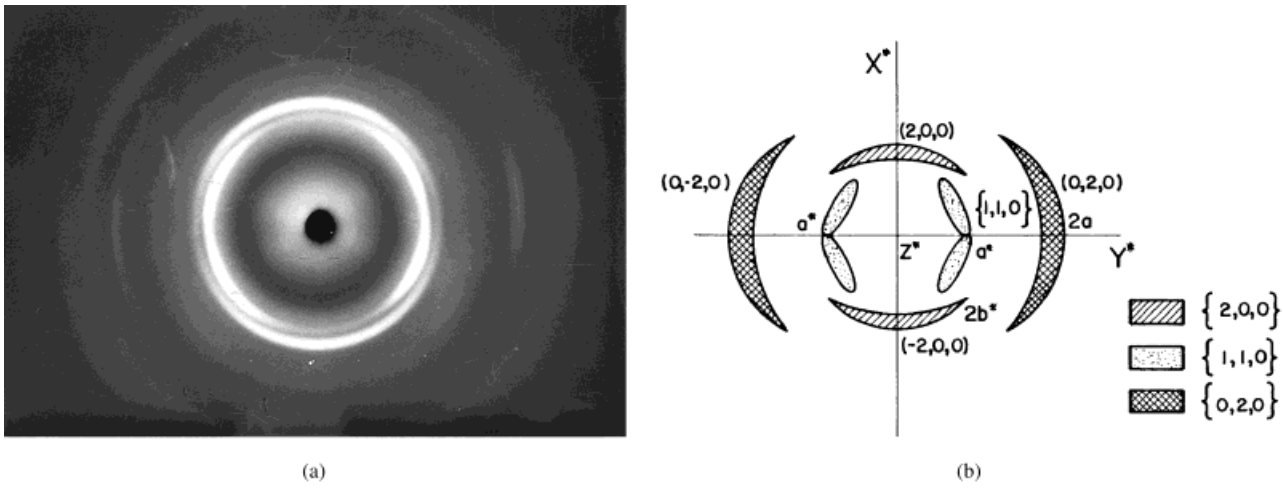

Figure 3 (a) Photograph of LDPE sample A, taken by wide angle X-ray spectrometry (WAXS). (b) Explanatory diagram of the above photograph, showing the arrangement of the different maximums for sample A, obtained by X-ray diffraction.

Table III Measurements of Maximum (2, 0, 0) and (0, 2, 0) the Corresponding Bragg Double Angles and the Parameters of the Real Unit Cell

Sample	$r_{(2,0,0)}$	$2\theta_{(2,0,0)}$	$r_{(0,2,0)}$	$2\theta_{(0,2,0)}$	a (Å)	b (Å)
A	18	24° 14′	29	36° 56′	7.51	5.14
B	17.5	23° 38′	29	36° 56′	7.69	5.14
C	17	23° 2′	30	36° 52′	7.88	5.14
D	17.2	23° 16′	29	36° 56′	7.81	5.14
E	17	23° 1′	27.7	34° 42′	7.88	5.42

Values of $r_{(i,j,k)}$ are expressed in millimeters.

direction Z, which is perpendicular to the surface of the film. In the present case, these functions are

$$f_\alpha = \frac{1}{2}[3(\cos^2\theta_{200}\overline{\sin^2}\phi_{200}) - 1], \quad (1)$$

$$f_\beta = \frac{1}{2}[3(\cos^2\theta_{020}\overline{\sin^2}\phi_{020}) - 1], \quad (2)$$

where

$$f_\alpha + f_\beta + f_\theta = 0 \quad (3)$$

Expression 3 provides the value of f_θ.

For this purpose the WAXS negatives were processed by photodigitalization scanning microdensitometry with a Perkin-Elmer model 1010 M apparatus (Norwalk, CT) to measure optical density $D(x, y)$ in squared microsurfaces of 2500 μm^2, along successive linear trajectories covering the whole surface in the first quadrant of these negatives. This procedure produced five files of grids having approximately 600 rows and 900 columns, each.

According to Stein,[21] the fundamental expression for the average value: $\overline{\sin^2}(\phi_{hkl})$ appears as the quotient of the two integrals:

$$\omega_1 = 4I_0 \int_0^{\pi/2} \int_{r_1}^{r_2} 10^{-D(r,\phi)} \sin^2\phi_{\mathrm{h,k,l}} \cos\,\phi_{h,k,l} r dr d\phi, \quad (4)$$

$$\omega_2 = 4I_0 \int_0^{\pi/2} \int_{r_1}^{r_2} 10^{-D(r,\phi)} \cos\,\phi_{h,k,l} r dr d\phi \quad (5)$$

Since, it was assumed that we were dealing with uniaxial elements, these integrals were calculated directly in cylindrical coordinates by numerical methods. The numeric problem was resolved on a digital VAX-9000 computer, using as software the Subroutines FORTRAN "IMSL MATH/Library." From there, the subroutine DQAND (Double Precision mode) was taken, which also provides an estimation of the absolute error.

TEM and Sample Preparation

Rectangles of 1 × 2 mm were cut out from samples A, B, C, D, and E, and these were included with Epon 812 in the same way as for biological samples.

Next, they were cut to expose the cross section of the film. The aforementioned ultramicrotome

Table IV Dimensions of Microdensitometry Files, Starting and Ending Limits of the Debye Circle (0, 2, 0) and Results of the Two Integrals, Eqs (4) and (5) and Their Quotient ≡ $(\overline{\sin^2}\phi_{020})$

Sample	File Dim.	r_1	r_2	ω_1	ω_2	ω_1/ω_2 (10^{-3})
A	623 × 966	560	600	5608 ± 49	15628 ± 87	359 ± 5
B	689 × 965	560	600	6008 ± 38	18054 ± 104	333 ± 4
C	633 × 906	540	600	9158 ± 03	25124 ± 16	364 ± 0
D	628 × 927	530	600	9756 ± 31	28444 ± 231	343 ± 4
E	675 × 939	530	580	7472 ± 53	20949 ± 71	357 ± 4

Table V Values of the Three Orientation Functions Corresponding to the Blown Polyethylene Samples

Sample	f_α (10^{-3})	f_β (10^{-3})	f_θ (10^{-3})
A	−500 ± 13	38 ± 4	462 ± 17
B	−500 ± 13	−1 ± 0	501 ± 13
C	−500 ± 13	47 ± 0	453 ± 13
D	−500 ± 13	14 ± 2	486 ± 16
E	−500 ± 13	35 ± 3	465 ± 15

Table VI Average Values of the Three Angles Formed by the Crystallographic Axes with the Direction of *Z* Axis

Sample	α (±1°)	β (±1′)	θ (±1′)
A	90°	53° 12′	36° 47′
B	90°	54° 46′	35° 13′
C	90°	52° 51′	37° 08′
D	90°	54° 09′	35° 50′
E	90°	53° 19′	36° 40′

was cut to thicknesses of between 800 and 1000 Å, and the samples were placed on a 400 mesh/mm^2 copper grid. Samples were observed and examined on a 200 kV Jeol model 2000-FX transmission electron microscope (Peabody, MA) with a maximum resolution of 1.4 Å between lines and 2.8 Å between points. Two series of samples were prepared, one without prior treatment and the other using the basic method described by Kanig[22,23] to achieve stability in crystalline structures by fixing their methyl radicals. This method consists of treating polyethylene samples with

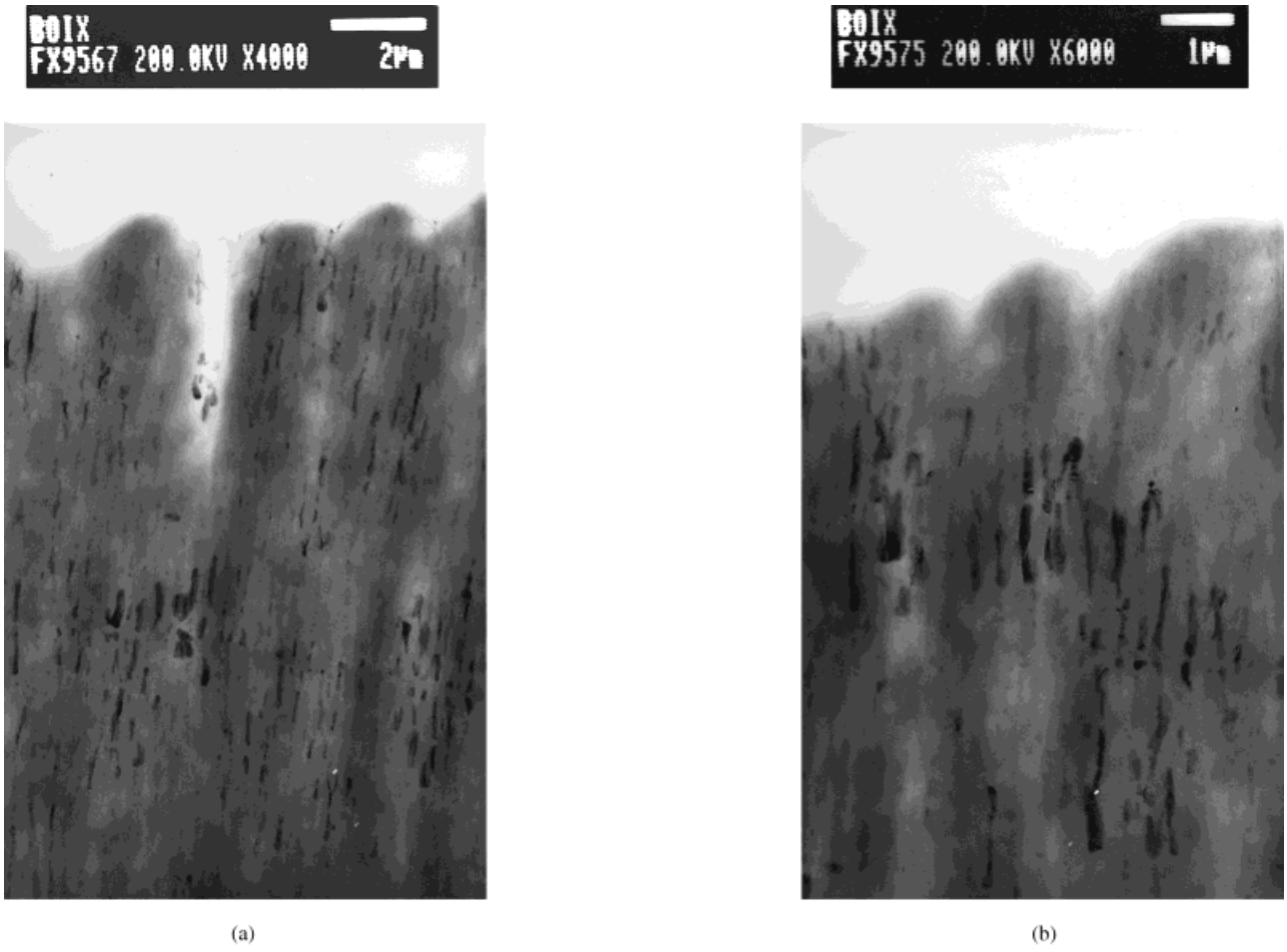

Figure 4 (a) Two photographs, taken by TEM, showing the appearance of the fibers. (b) (2–3 μm) perpendicular to the film surface. (Photographs taken of untreated LDPE samples).

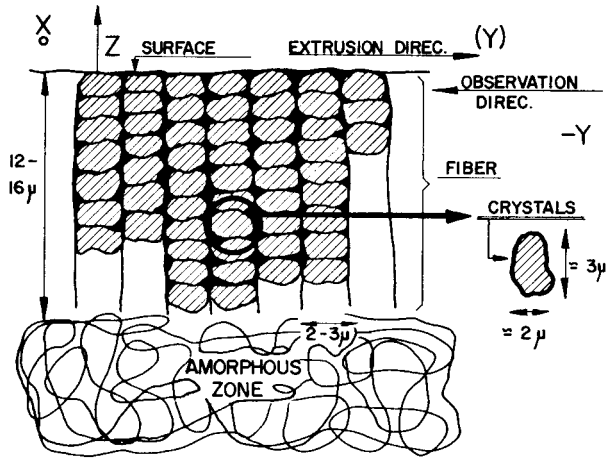

Figure 5 Diagram showing arrangement of crystals inside fibers, with the long crystal axis lying parallel to the surface in the extrusion direction from which a crystal was extracted for analysis.

chlorosulphonic acid for 16 h, which darkened considerably by the end of this period.

MICROSTRUCTURAL DESCRIPTION AND RESULTS OF MICROSCOPY

Determination of the Third Refraction Index and Structure Characterization by POM

The results of the procedures described in Polarized Optical Microscopy are shown in Table I. According to Buttgenbach,[24] the n value of the third index for optically negative crystalline elements can be obtained by

$$n_\alpha = n_\gamma - \frac{n_\gamma - n_\beta}{\sin\left(V_\alpha \dfrac{\pi}{180}\right)} \tag{6}$$

The values of $n_\gamma \equiv n_0$ and $n_\beta \equiv n_e$ coincided with those determined previously for the same material by Bernabeu et al.[25] In the case of sample A, the rule generally adopted in crystallography, whereby $n_\gamma > n_\beta$, did not hold. Thus, biaxiality was taken to be antinegative. Substitution of n_γ and n_β in expression (6), along with the values of angle V_α taken from Table I, resulted in the values of n_α. The final results are shown in Table II.

These three values of the refraction index and their linear fittings, f_1, f_2, and f_3, calculated as a function of the crystallinity degree, are plotted in Figure 1. The linear fit of f_2 and f_3 is significant, but that of f_1 is less clear.

POM procedures were used for the analysis of the 2-μm-thick cross section [Fig. 2(a)]. This shows a sandwich structure consisting of a thicker, amorphous middle layer, with a thinner crystalline layer on either side [dimensions shown in Fig. 2(b)]. Its origin and anisotropy were attributed to viscosity occurring upon pouring, as the melt emerges from the extruder nozzle (*birefringence d'écoulement*).[26] The difference in thickness between crystalline layers was due to different rates of cooling. The inner face cooled faster, owing to the flow of cold air injected into the middle part to form the blowing bubble. This hindered crystallization, making thickness less, whereas the outer face, which was in contact with the warmer room temperature air, cooled more slowly and thus thickened more.

Experimental Results of X-ray Diffraction

Following the procedure described in Polarized Optical Microscopy a series of five photographs were obtained, one for each sample, similar to those for sample A in Figure 3(a). Results presented in graphic form for analysis according to ref. 27 are shown in Figure 3(b). From these, the {1, 1, 0} family of crystallographic planes was placed in the central area. The presence of "crescent moon"–shaped peaks indicates diffraction by imperfectly aligned microcrystals. In the second circle, there are two peaks situated at 90° and 270°, corresponding to the {2, 0, 0} family of planes, from which the value of a^* along the X^* axis can be determined.

About 30 mm from the center (measured on the negative side of the scale indicated), there is a fourth ring, also of interest, representing the {0, 2, 0} family perpendicular to the Y^* axis, from which the value of b^* can be calculated.

Briefly, this is a diffraction diagram of a film of partially crystalline material belonging to the orthorhombic system, taken perpendicular to the surface in the direction corresponding to the Z^* and Z axis,[27] since it is considered to be uniaxial. These results were used to calculate the real values of crystalline parameters a and b of the unit cell in each polyethylene sample. Results are shown in Table III.

Orientation Functions: Results

Using the method described in X-ray Diffractometry, the values of the orientation functions

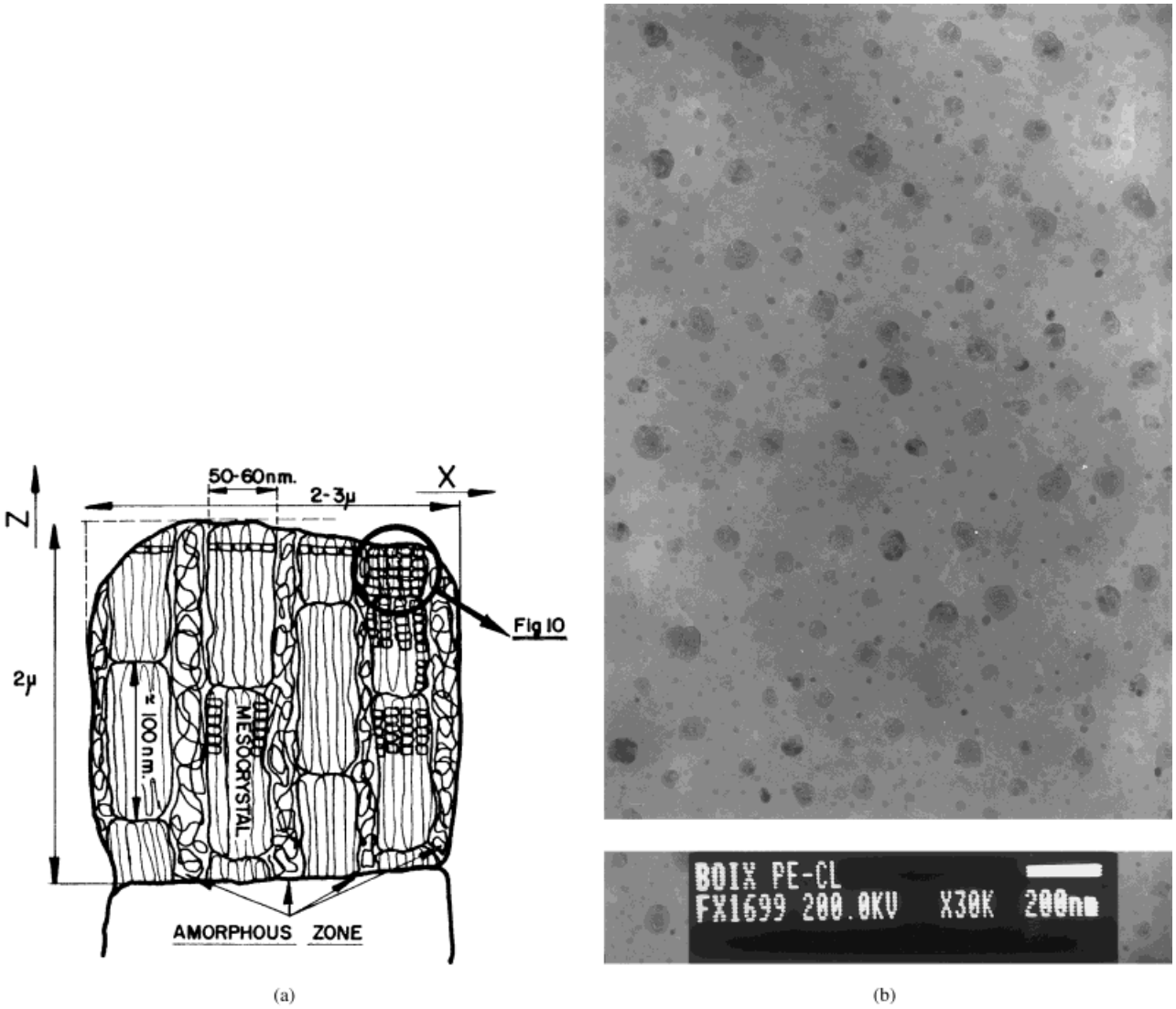

Figure 6 (a) Schematic drawing showing the make-up of a typical crystal, composed of mesocrystals, viewed counter to the extrusion direction. Detail taken from the interior for analysis. (b) Spatial mesocrystal aggregate, size approx. 100 nm, probably produced by the action of chlorosulphonic acid on fiber crystals.

needed to build our model were derived, since it was necessary to ascertain the real situation of the "average unit cell" inside the material as precisely as possible. It has been shown that for all samples, the respective Bragg angle $\theta_{200} = \pi/2$ with respect to the X axis, if we take the expression f_α in eq. (1). This implies that $f_\alpha = -1/2$. For the (0, 2, 0) plane corresponding to function f_β, the corresponding Bragg angle $\theta_{020} \cong 0$ with respect to the same origin. According to Stein,[21] this confirms that $\cos^2\beta \cong \overline{\sin^2}\phi_{020}$. In this case, to obtain its value, the integration procedures previously referred to must be applied. To determine the radial integration limits r_1 and r_2, the distances from the center to each of the boundary circles were measured in millimeters. Then, the column order corresponding to each radius was obtained, dividing by 50. The data for all these operations and procedures are given in the first four columns of Table IV. The partial results are shown in the three columns on the right. The quotient of ω_1/ω_2 substituted in expression (2), provides the values of f_β and herefrom the values of f_θ can be derived by applying the general property (3). Results are shown in Table V.

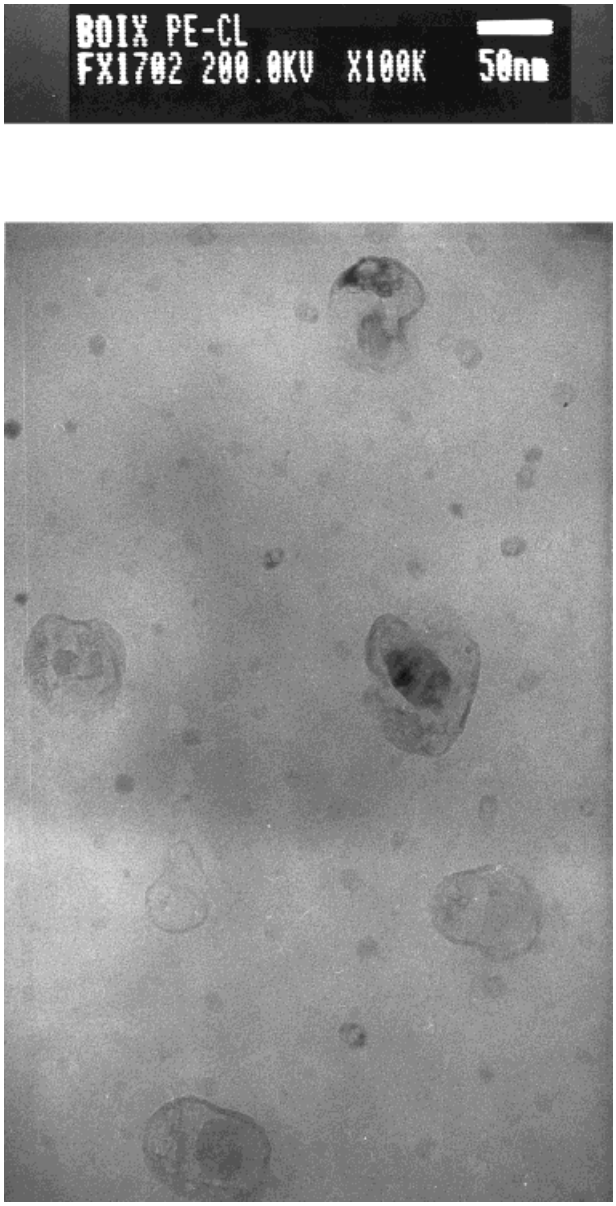

Figure 7 Further enlarged photograph of a mesocrystal. Electron diffraction carried out on central zone.

With these results, a number of general consequences can be derived with regard to the position of the crystallographic axes in the reciprocal space and hence the values of their corresponding numbers in real space. Thus, the constant value of f_α equal to -0.5, means that crystallographic axis x_a^* is perpendicular to axis Z^*, and hence x_a in real space will be perpendicular to reference axis Z and parallel in turn to axis X. Finally, once the value of α = constant is known, the mean values of angles β and θ also can be calculated. All these results are shown in Table VI.

The following physical microstructural consequences follow from the values of the orientation functions. With respect to the angle α, it follows that axis X_a is perpendicular to axis Z, and hence, this will be the direction of edge a of the unit cell, which consequently also will be parallel to the surface of the film. Since y_b is almost totally random, with respect to angle β, according to Stein[21] total randomness occurs for $f_{\phi T} = 0$; this means that $\overline{\phi_T} = 54° 44'$. Therefore, the angles β differ from this by $\pm 1° 30'$ at the most. However, this randomness on axis y_b implies further randomness on the third axis z_c with respect to Z, since θ angle is complement of β. Hence, $\overline{\theta_T} = 36° 16'$.

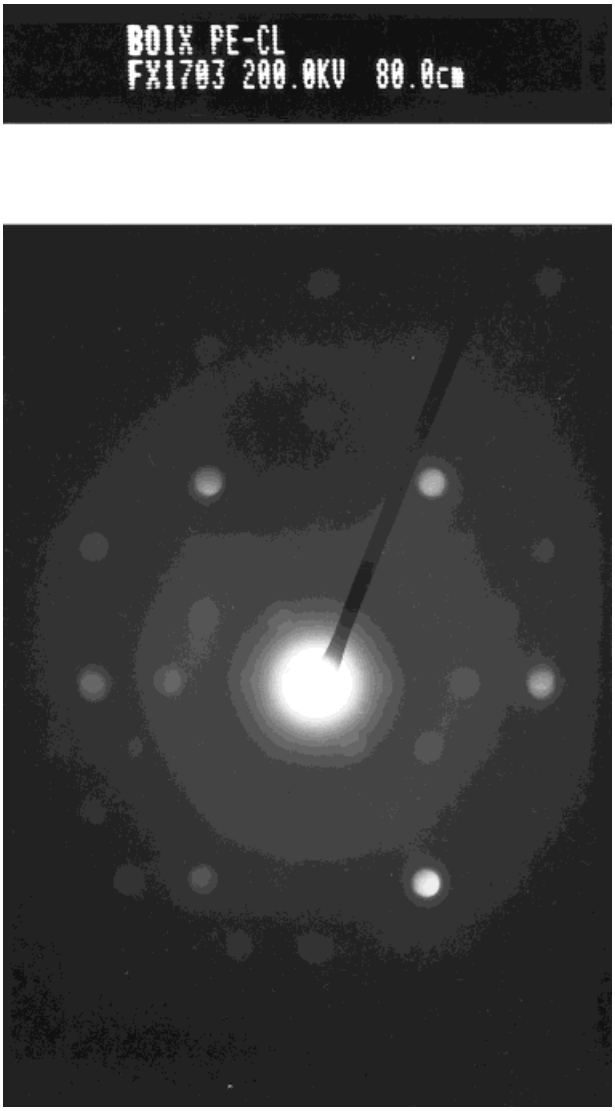

Figure 8 Photograph showing the result of electron diffraction on a mesocrystal, confirming its crystalline structure.

Microstructural Approach and Justification by TEM

In order to develop a microstructural model, it must be taken into account that as a result of the pouring process (écoulement),[26] crystal aggregates as photographed by TEM appear arranged in such a way as to form a series of quasi-cylindrical structures. These are known as fibers and are approximately 2–3 μm in diameter [Fig. 4(a,b)]. This occurred without any prior treatment of the polyethylene. It was these crystals that formed the crystalline parts of the sandwich structure described earlier. A diagram of the fibers (Fig. 5) shows interior crystal disposition in a "pills in a tube" arrangement, the major axis being parallel to the surface.

If we now change the direction of observation to the axis *Y* (counter to the extrusion direction), we can see from the diagram in Figure 6(a) that each crystal was composed of other, smaller elements. These shall be called *mesocrystals,* and they are 50–60 nm broad and about 100 nm long, arranged in columns and separated by other amorphous zones 20- to 25 nm thick. Experimental confirmation of the existence of these mesocrystals may be drawn from Figure 6(b), which shows a group of elements of this kind, possibly isolated by the action of chlorosulphonic acid[27,28] and hence, more easily visible. Figure 7 shows an enlarged mesocrystal that was subjected to electron diffraction to demonstrate its crystalline character (Fig. 8).

Part of the mesocrystal diagram [Fig. 6(a)] was extracted for enlargement in order to examine its interior. This revealed a *lamellar structure* (Fig. 9) in which a set of isolated, linear lamellae were apparent. From this photograph, measurements were taken of the crystalline and amorphous zones, from which it was possible to estimate what is known as lamellar crystallinity; in the present case, this was 44%.

The diagram in Figure 10 shows the crystalline zones made up of blocks (of approximately 100 microcrystals each), roughly 10^3 Å long and 22–25 Å wide, called *crystallites.* These were separated by semi-orientated (anisotropic) or mesomorphic zones, 28–30 Å thick on average, bounding the amorphous zone, in such a way that the chains followed the direction of the *Z* axis and were therefore, perpendicular to the surface. The sides of the amorphous zone, known as trans-crystalline zones, were more ordered. In the area of the boundary with the crystals, there were paracrystalline zones, which became progressively less ordered toward the center of the amorphous zone, followed by amorphous zones having a some orientation (amorpho-anisotropic zones), whose percentage values were previously calculated.[29]

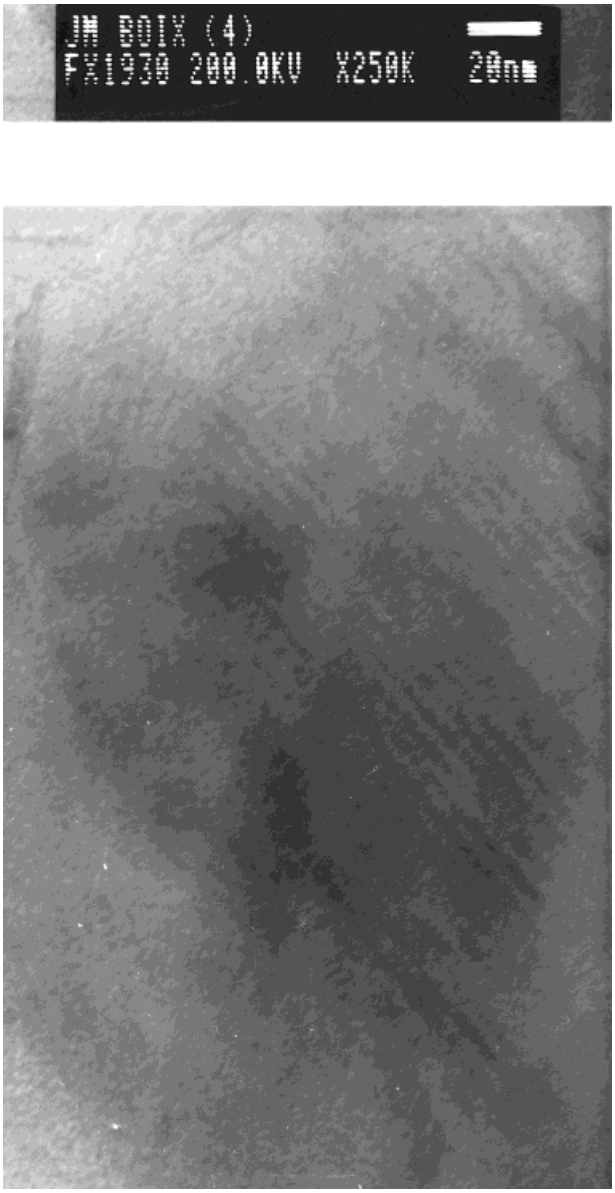

Figure 9 Photograph showing a group of linear and parallel lamellae, whose measurements can be used to calculate the lamellar crystallinity value for a sample of low-density blown polyethylene.

The microcrystals in the first column, running from the central amorphous part to the surface, were composed of five polymer chains [see Fig. 10], constituting what we have called a *microfiber.* To further clarify this structure, an enlargement is shown in Figure 11. It should be noted

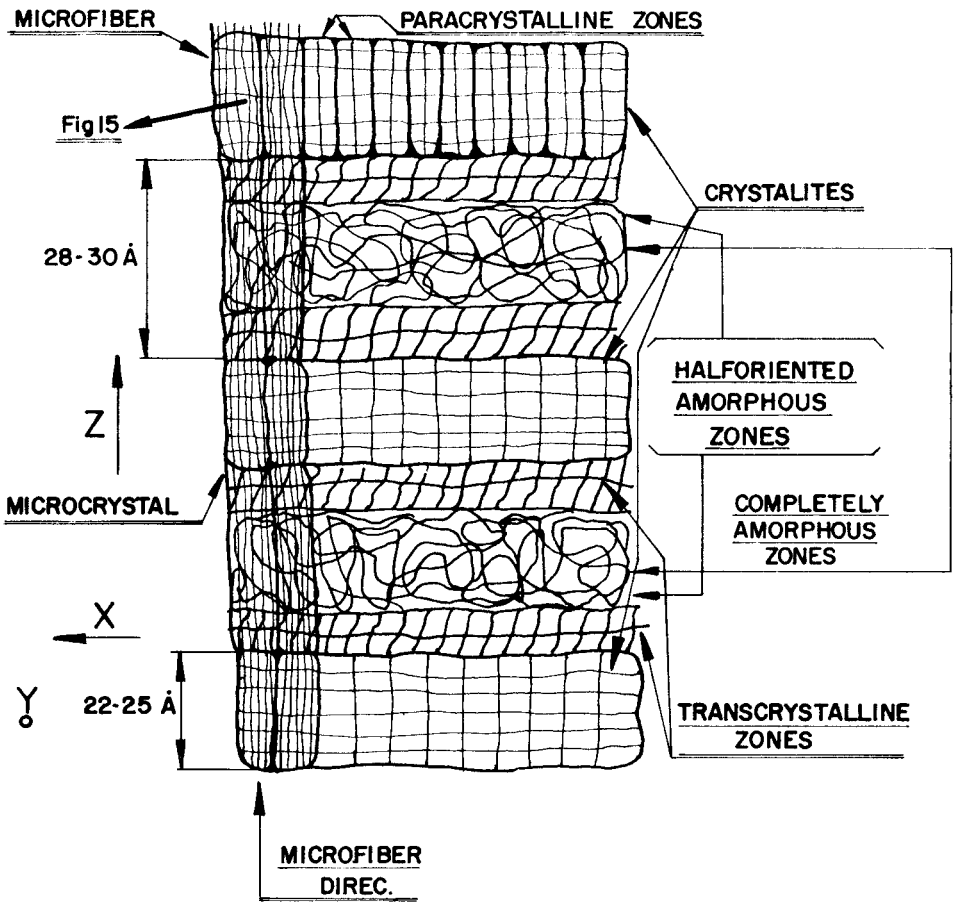

Figure 10 Diagram of a lamellar zone, taken from part of Figure 6(a), clearly showing all components and sizes.

that these were not isolated, but were interlinked according to the models proposed by Flory[30] and Kanig.[23]

Finally analyzed was the fundamental element of the microfiber, which we designated as the *microcrystal*. As the diagram in Figure 12(a) shows, it was composed of 9 or 10 orthorhombic cells [shown in Fig. 12(b)], positioned as follows: side c lay along the Z axis, perpendicular to the film surface; side b lay along the Y axis or extrusion direction (MD in some texts); side a lay along the X axis (TD), and hence almost parallel to the surface, in an ideal situation. This coincides exactly with the refraction indices measurements made on an Abee refractometer,[25] as well as being consistent with the diagrams of X-ray diffraction and calculations of their orientation functions.

OPTICAL MICROSTRUCTURAL MODEL

Our aim was to set up a model, consistent with the microstructure of the material, to explain the optical properties examined earlier,[25,29] in blown, low-density polyethylene films samples.

To do this, an indicatrix surface (or index ellipsoid) was inscribed inside an orthorhombic crystallographic cell (see Fig. 14) with some modifications. This was done to explain its behavior as a polymer with optical properties, strictly in accordance with previously described microstructural characteristics. Since the refraction index values were very close in the present case (Table II), the indicatrix surface was a spheroid. To inscribe the electromagnetic spheroid, the following parameters were taken as distances from the sides forming the electromagnetic cell or active structure when this is traversed by electromagnetic radiation: ($c_{\text{E-M}} = 2c$, $b_{\text{E-M}} = b$ and $a_{\text{E-M}} = 2a/3$, where a, b, and c are the values calculated in our unit cell). The behavior of polymeric material was that of a cell twice the height $2c$, the same width b, and two thirds of the length $2a/3$. This is as if there were two "virtual" walls, each side being displaced by a distance $a/6$. (The term "wall" re-

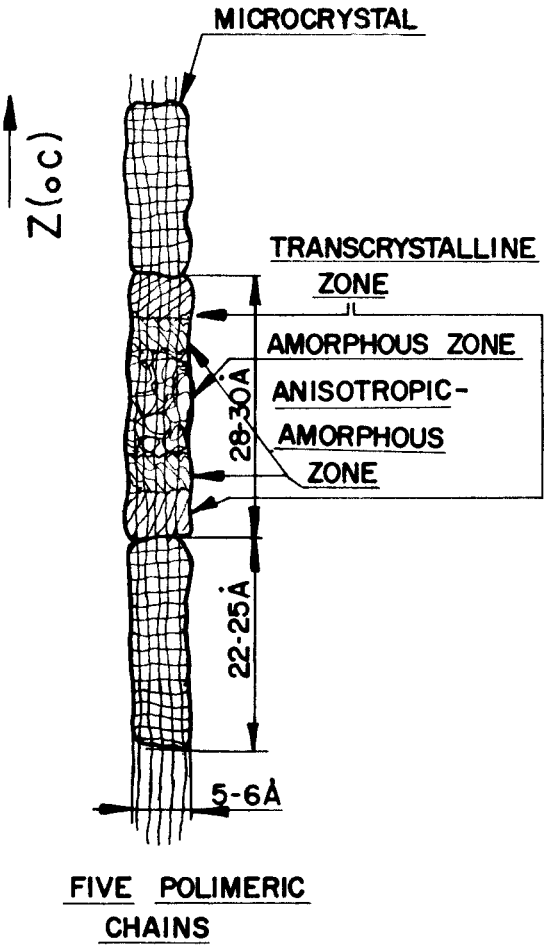

Figure 11 Diagram showing the enlargement of a microfibre, with its various parts: crystalline, microcrystals; amorphous, anisotropic; totally amorphous.

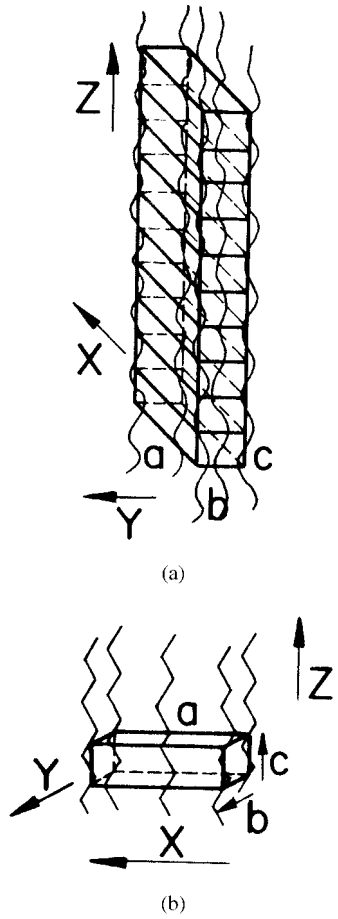

Figure 12 (a) Make-up of a microcrystal composed of orthorhombic unit cells. (b) Detail of an isolated unit cell in relation to the sample's system of axes.

fers here to a nonexistent geometrical-physical boundary linking four dipoles located at the four vertices, which symbolizes the action of the resulting field.) These two walls, although not physically present, cause the material to behave for the purposes of electromagnetic waves, as if they were so arranged. A possible empirical justification for this change in length of the orthorhombic cell is that the dipolar fields in the unit cell referred to are disturbed by the passage of electromagnetic radiation.

Figure 13 shows how a simple proportion was established between the semi-axes represented by the refraction indices and the respective semisides of the orthorhombic electromagnetic cell, that is,

$$\frac{3n_\gamma}{a} = \frac{2n_\beta}{b} = \frac{n_\alpha}{c} = r \qquad (7)$$

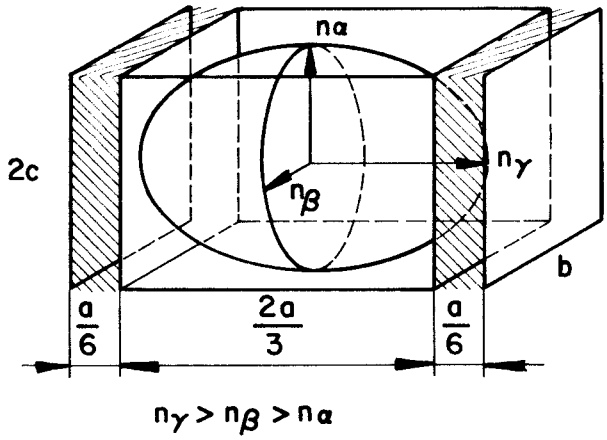

Figure 13 Diagram showing the make-up of the electromagnetic cell, which is the basis of our model. Taken from a negatively biaxial crystal.

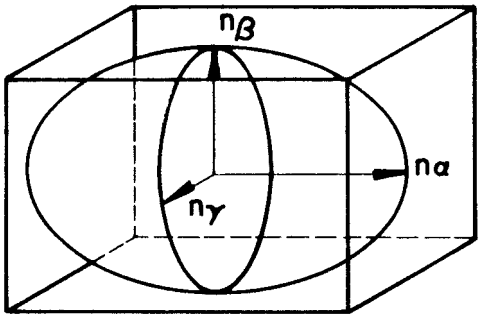

Figure 14 Schema showing another type of electromagnetic cell, in this case belonging to antinegative biaxial crystalline elements of low-density blown polyethylene.

which we take as corresponding to negative biaxiality. This is the case in all the samples in Table II, except for the first, sample A, designated as anti-negative, in which the above relationship holds, but with the last two denominators reversed

$$\frac{3n_\gamma}{a} = \frac{n_\beta}{c} = \frac{2n_\alpha}{b} = r' \tag{8}$$

Thus, the inversion of biaxiality is justified (Fig. 14). In other words, with respect to Figure 13, the three axes have undergone a 90° turn (circular permutation), but the relative position of the figure as a whole inside the material remains the same.

Regarding the most probable orientation inside the sample with reference to the axes (X, Y, Z), on the basis of the calculated values of the orientation functions and the conditions described in the previous section, the spatial distribution shown in Figure 15 was developed.

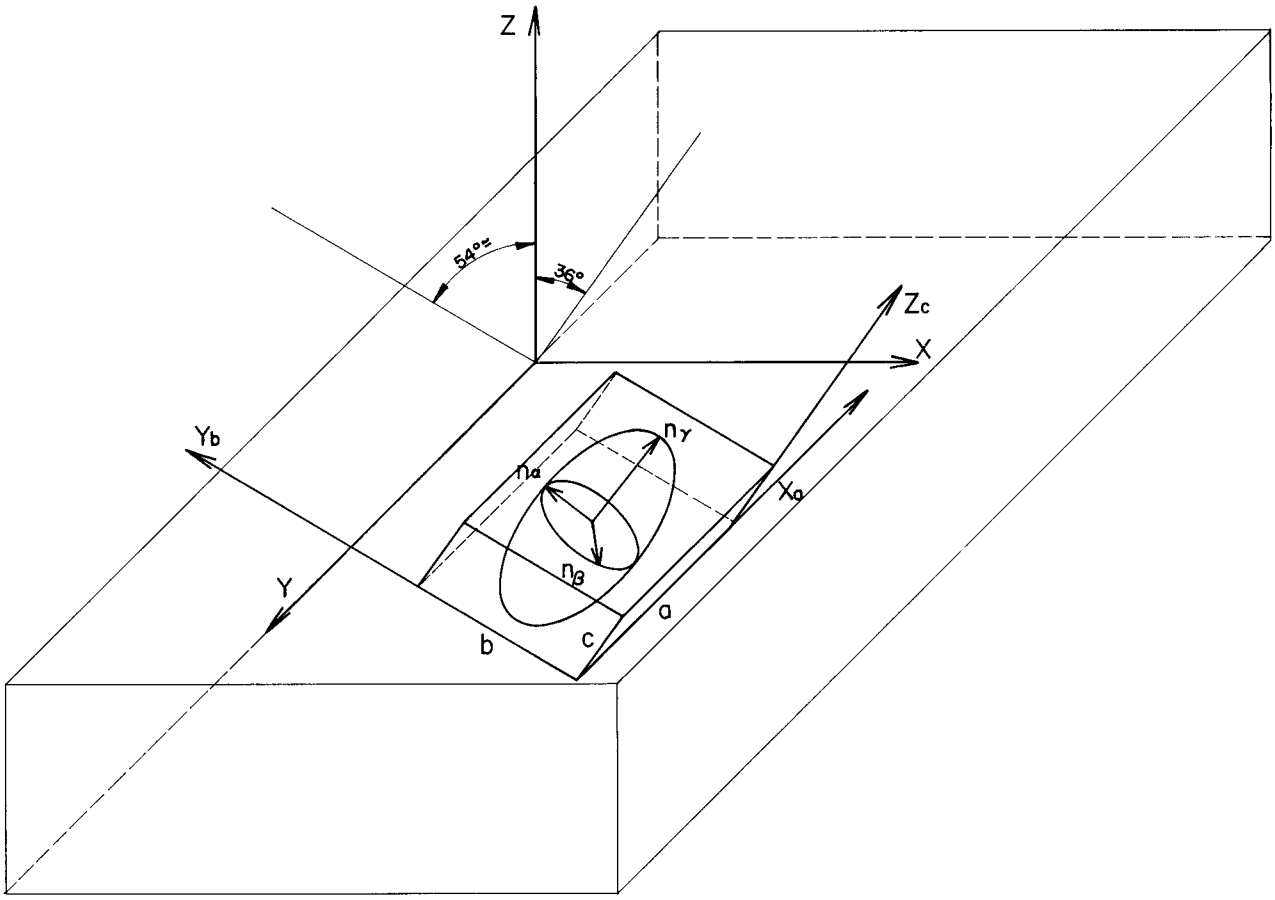

Figure 15 Diagram showing the most probable random position, inside the sample, of the cell on which the optical-microstructural model is based, according to the results of the orientation functions.

Table VII Ratio Values of Expressions (7) and (8), and Their Absolute Errors, with the Crystallinity Degree for the Five Samples Studied

Sample	X_c	$r\ y\ r'$	Absolute Error
A	31.5	0.60 (r')	$\pm 4 \times 10^{-3}$
B	44.9	0.59	$\pm 3 \times 10^{-3}$
C	45.6	0.59	$\pm 4 \times 10^{-3}$
D	47.1	0.59	$\pm 5 \times 10^{-3}$
E	49.1	0.57	$\pm 1 \times 10^{-2}$

Now the values of a and b derived from the results of the X-ray diffraction diagrams (Table III) and $c = 2.53$ Å from ref. 31, were applied to expression (7) for samples B, C, D, and E (The slightly larger error shown by E is due to a larger value of b). With the values in sample A verified by eq. (8), the proportions were shown to be constant for all cases, as the final results show in Table VII. The consistency of these values confirms the validity of our model.

CONCLUSIONS

The main purpose of this work was to establish a model for blown low-density polyethylene films to explain the fundamental optical properties exhibited by this type of polymeric laminates (refraction, birefringence, and anisotropy). This was done by microstructural examination with TEM and X-ray diffraction, from which the values of its orientation functions were calculated.

In this way it was possible to inscribe a Cauchy spheroid inside the electromagnetic cell, which was sufficient in itself to explain the behavior of LDPE as an optical polymer. The model may be considered a weakly oriented semi-crystalline structure, with crystals distributed randomly in number and position, for which only mean values are found. We may thus conclude, that material so structured is only locally homogeneous and that in spite of its heterogeneousness, the overall appearance of the material is that of a stable, perfectly integrated whole, with definite properties, just as if it were a product of nature.

REFERENCES

1. Schael, G. W. J Appl Polym Sci 1964, 8, 2717.
2. Schael, G. W. J Polym Sci 1968, 12, 903.
3. de Vries, A. J., et al. J Polym Sci Polym Symp 1977, 58, 109.
4. de Vries, H. Thesis, Delf, 1953.
5. de Vries, H. J Polym Sci 1959, 34, 761.
6. de Vries, H. Angew Chem 1962, 74, 574.
7. de Vries, H. Coll Polym Sci 1979, 257, 226.
8. de Vries, H. Coll Polym Sci 1980, 258, 1.
9. Wedgeweood, A. R.; Seferis, J. C. Polym Eng Sci 1979, 19, 975.
10. Samuels, R. J. J Appl Polym Sci 1981, 26, 1383.
11. Cakmak, M.; Spreuiell, J. E.; White, J. L. S.P.E. ANTEC 1983, 29, 394.
12. Cakmak, M. Ph.D. Thesis, University of Tennessee, Knoxville, TN, 1984.
13. Snow, B. D.; Moore, J. T. S.P.E. ANTEC 1984, 30, 504.
14. Jabarin, S. A. Polym Eng Sci 1984, 24, 376.
15. Guan, J. Y.; Saraf, R. F.; Porter, R. S. J Appl Polym Sci 1987, 33, 1517.
16. Janeschitz-Kriegl, H.; Wales, J. L. S. Nature 1967, 213, 1116.
17. Morton, W. E.; Hearle, J. W. S. Physical Properties of Textile Fibers; Textile Institute and Butterworth: London, 1962.
18. Simmers, S.; Hearle, J. W. S. J Polym Sci Phys Ed 1980, 18, 871.
19. Tsvetkov, V. N.; Andreeva, L. N. Polymer Handbook; Brandrup, J.; Immergut, E. H., Eds.; 2nd. ed. IV. 377. Wiley: New York, 1975.
20. Pinto, G. Ph.D. Thesis, Universidad Complutense. Madrid, Spain, 1990.
21. Stein, R. S. J Polym Sci 1958, 31, 327.
22. Kanig, V. G. Kolloid Z und Z Polymere 1973, 251, 782.
23. Kanig, V. G. Prog Colloid & Polymer Sci 1975, 57, 176.
24. Buttgenbach, H. "Cours d'Optique Cristalline." Dunod ed.; Paris, 1936.
25. Bernabeu, E.; Boix, J. M.; Larena, A.; Pinto, G. J Mat Sci 1993, 28, 5826.
26. Bruat, G. "Optique," 5th ed.; Masson & Cie: Paris, 1965.
27. Kakudo, M.; Nasay, N. "X-Ray Diffraction by Polymers." Kodansha, Ed.; Lda & Ensevier Publishing Com.: New York, 1972.
28. Martinez-Salazar, J.; Rueda, D. R.; Cagiao, M. E.; Lopez-Cabarcos, E.; Baltá Calleja, F. J. Polymer Bulletin 1983, 10, 553.
29. Larena, A.; Pinto, G.; Bernabeu, E.; Boix, J. M. Polym-Plast Technol Eng 1994, 33, 551.
30. Flory, P. J. Nature 1978, 272, 226.
31. Zugenmaier, V. P.; Cantow, H. J. Kolloid Z und Z Polymer 1969, 230, 229.